Interaction- and measurement-free quantum Zeno gates for universal computation with single-atom and single-photon qubits

Y. P. Huang and M. G. Moore

Department of Physics & Astronomy, Michigan State University, East Lansing, Michigan 48824, USA

By extending the concept of interaction-free imaging to the few-atom level, we show that asymptotically on-demand interaction- and measurement-free quantum logic gates can be realized for both single-atom and single-photon qubits. The interaction-free feature suppresses the possibility of qubit decoherence via atomic spontaneous decay, while the elimination of measurements can significantly reduce errors arising from detector inefficiency. We present a general theory of universal quantum Zeno gates, and discuss physical implementations for quantum-information processing with individual atoms and photons. In addition, we propose a loss-tolerant protocol for long-distance quantum communication using quantum Zeno gates incorporated into a Mach-Zehnder interferometer. The efficiency of our Zeno gates is limited primarily by the imprecise control of atom-photon scattering and the finite number of feedback cycles N due to the limited finesse of the optical ring cavity. We find that the success probability scales as $1 - O(1/N)$, and for realistic parameters could be as high as 98.4%. Successful generation of atom-atom entanglement can be heralded by detection of the ancillary photon, upon which the fidelity scales as $1 - O(1/N^2)$, with an achievable fidelity of 99.994%, which comes at the cost of reducing the success probability by the detector efficiency.

PACS number(s): 03.67.Lx, 42.50.Ex, 42.50.Dv

I. INTRODUCTION

The past decade has seen steady experimental progress in realization of quantum-information-processing protocols [1], including those for quantum computation [2–11], quantum communication [12–14], quantum cryptography [15], quantum dense coding [16], and optimal phase estimation [17]. The systems used in these experiments have involved purely photonic qubits [18], mixtures of atomic and photonic qubits [19–22], or purely atomic qubits [23–25], where "atomic" here refers to any massive particle or ensemble of massive particles. One of the challenges faced in mixed-qubit applications is to create strong coherent interactions between atomic and photonic qubits. If achieved, this could lead to two-qubit operations between remote atomic qubits via a common photonic channel, thus eliminating the restriction to nearest-neighbor interactions when processing an array of atomic qubits.

A typical scheme for such entanglement generation would involve passing over both atomic qubits a far-detuned light pulse, whose polarization interacts only with one of the qubit internal states. Detection of a certain phase shift in the light pulse relative to an idler pulse could indicate that one of the qubits was in the interacting state, but not which one, thus collapsing the two-qubit state into an entangled state [26,27]. While a light pulse containing many photons can have a strong effect on a single atom, the back effect of the atom on the light field is very small. The primary difficulty in creating entanglement between two atomic qubits via a common photonic channel thus lies in the need to employ a sufficiently large number of photons to detect the small phase distortion generated by a single atom, while avoiding the loss of information due to atomic spontaneous decay and/or imperfect optics. This problem is typically addressed by using high-finesse optical cavities to enhance the coupling while reducing the spontaneous decay [28,29], and/or replacing single-atom qubits with collective ensemble qubits [26,30,31]. With atomic ensemble qubits, however, the coherence time will be limited by information-destroying short-range interactions (collisions). In order to avoid this limitation, one can use single isolated trapped atoms, which then requires a high-finesse optical resonator in the strong-coupling regime, and/or the use of highly nonclassical light pulses [27].

In cavity QED approaches, one usually seeks to suppress spontaneous emission by significantly decreasing the density of states of the electromagnetic vacuum, so that a coherent atom-photon interaction becomes possible over some time-scale. Despite the widely held belief that decoherence must always be avoided in quantum-information processing, it has been known for some time that decoherence can instead be harnessed to implement high-efficiency coherent quantum logic gates for single photons and atoms [32]. These gates rely on the fact that strong coupling to the environment is equivalent to continuous measurement, and can therefore inhibit coherent quantum dynamics, in analogy with the quantum Zeno effect [33–38]. To best understand how such an effect can lead to coherent entanglement generation, consider a set of experiments where the Zeno effect was used to allow a single photon to image an absorbing object without being absorbed, known as high-efficiency interaction-free measurement (IFM), or alternatively as "quantum interrogation" [39–45]. Replacing the classical absorber with an atomic qubit, prepared in a superposition of absorbing and transparent states, can coherently change the quantum state of the probe photon conditioned on the state of the atomic qubit [46]. This leads to atom-photon entanglement, generated via a mechanism in which the atom and photon arguably never interact directly, so that spontaneous emission (decoherence) is avoided even for a resonant photon. In such a system it is simply the possibility of a strong dissipative interaction which drives the Zeno effect and creates entanglement, without dissipation actually occurring. The Zeno effect forces the

system to remain in a decoherence-free subspace (DFS) [47–49], and thus greatly suppresses the possibility of decoherence via spontaneous decay.

Several schemes for quantum entanglement manipulation and/or gate operation via IFM have been recently proposed [50–54]. Utilizing the dissipative photon-atom interaction, Gilchrist *et al.* propose implementing conditional, postselection protocols to generate Bell-, W-, and Greenberger-Horne-Zeilinger- (GHZ-)type states for single atoms with a maximum success probability of 1/4 [50]. They also provided an approach to generate an *n*-photon superposition state with *n* IFM devices aided by an ancillary atom, where the final atomic state is measured and a logical operation is performed conditioned on the measurement outcome. In a closely related work, Azuma proposed to generate Bell states of an electron-positron pair, where pair annihilation supplies the equivalent dissipative interaction to drive the Zeno effect [51]. Also demonstrated for such a system are a Bell-measurement circuit and a controlled-NOT (CNOT) gate, with maximum success probabilities of 3/4 and 9/16. By chaining multiple IFM devices, Azuma was able to further push the success probability of the Bell-measurement circuit and consequently the CNOT gate to be near unity [52]. This CNOT gate requires four ancillary entangled qubits, two Bell measurements, together with four classical measurements and multiple measurement-conditioned operations. This is arguably too complex a construction relative to the simplicity of the task. In a non-IFM-based yet related approach, Franson *et al.* proposed using the quantum Zeno effect to inhibit more than one photon occupying the same optical fiber mode, and thus implement the $\sqrt{\text{SWAP}}$ gate between two photonic modes, leading to subsequent improvements in quantum computing with single photons [53]. Also very interestingly, using the "chained" quantum Zeno effect, Hosten *et al.* demonstrated *counterfactual* quantum computation, where the potential outcome of a quantum computation can be inferred without actually running the computer [54].

In this paper, we consider three important changes to the standard IFM gate which allow us to design an extremely simple and elegant set of quantum logic gates toward quantum-information processing. First, in contrast to simply flipping the internal state of the probe qubit, we allow arbitrary state rotation of the probe qubit. Second, in addition to the usual IFM gate with a photon as the probe and atom as the object, we construct a complementary gate where the roles of atoms and photons are exchanged. Third, we consider placing multiple qubits in a single IFM circuit. With these changes, we are able to construct interaction- and measurement-free quantum logic gates in a straightforward manner.

We begin by presenting a generalized theory of the operating principle, and then consider physical implementations of such Zeno gates. Specifically, we design atom-photon, atom-atom, and photon-photon CNOT gates, as well as atom-to-photon and photon-to-atom state transfer circuits. We also consider a long-distance quantum communication protocol which is tolerant to photon transmission losses. All of our quantum Zeno gates are high efficiency in the sense that they deviate from unit success probability by a factor $\sim \frac{1}{N}$ and from unit fidelity upon heralded success by only $\sim \frac{1}{N^2}$. Here

N is the (effective) measurement number, limited only by technical considerations. One interesting feature of our design is that the IFM probe qubit acts only as an ancillary qubit, which is disentangled from the logical qubits at the end of the gate operation, so that no measurement of this qubit is required. The elimination of this measurement greatly boosts the success probability by removing errors due to detector inefficiency, as opposed to several previous schemes [1,5,8,11,19,22,55]. On the other hand, detection of the ancillary qubit in the output channel would herald successful gate operation, thus improving the fidelity of state creation by an additional factor $1/N$. In this way one can trade off success probability for fidelity, where success probability is decreased only by the detector inefficiency. As is typical in cavity QED applications, the trade-off for high fidelity is gate speed, as increasing *N* necessarily slows down the gate operation.

The organization of the paper is as follows. In Sec. II, we describe the general theory of quantum Zeno gates. In Sec. III, we present the physical implementations of two elementary Zeno gates built on the dissipative interaction between photons and atoms. Then, in Sec. IV we construct atom-atom and photon-photon CNOT gates, as well as a hybrid atom-photon phase gate. In Sec. V, we build atom-to-photon and photon-to-atom state transfer gates. In Sec. VI we then provide two long-distance quantum communication protocols, the latter of which is tolerant to photon loss. Lastly, we analyze the realistic success probability and the corresponding fidelity upon heralded success of the present quantum Zeno gates in Secs. VII and VIII, followed by conclusions in Sec. IX.

II. QUANTUM ZENO GATE: GENERAL THEORY

The quantum Zeno effect occurs when a rapid sequence of strong measurements is performed on a slowly evolving quantum system, with the result that the system is "frozen" in its initial state, i.e., the quantum watched pot boils more slowly than the unwatched pot. In the standard quantum Zeno effect, a two-level system (with states denoted $|0\rangle$ and $|1\rangle$) is rotated by a sequence of *M* rotations, each of angle θ/M. In the absence of measurements, this results in a net rotation of θ, so that a system initially prepared in state $|\Psi_i\rangle = |0\rangle$ is transformed to the superposition state $|\Psi_f\rangle = \cos\theta|0\rangle + \sin\theta|1\rangle$. The Zeno effect occurs when the system is measured in the $\{|0\rangle, |1\rangle\}$ basis after each θ/M rotation. It is readily found that the probability to find the particle in state $|0\rangle$ after *M* cycles is [33–36]

$$P_0 = [1 - \sin^2(\theta/M)]^M \approx 1 - \frac{\theta^2}{M}. \qquad (1)$$

This probability approaches unity in the limit $M \to \infty$, so that the system remains frozen in the initial state.

An analogous effect occurs in the case of a two-level system evolving under continuous coherent evolution and dissipation, as illustrated in Fig. 1. The coherent evolution is governed by the Hamiltonian
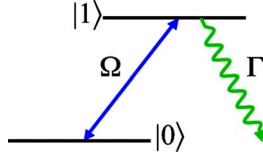
FIG. 1. (Color online) Level scheme for a two-state system with coherent coupling at Rabi frequency Ω and upper-state decay at rate Γ.

$$\hat{H}_\Omega = \frac{\hbar\Omega}{2}\sigma_y, \tag{2}$$

where σ_y is a Pauli spin matrix in the y direction. In the absence of dissipation, a system prepared initially in the state $|\Psi(0)\rangle = |0\rangle$ evolves after time t into the superposition state

$$|\Psi(t)\rangle = \cos(\Omega t/2)|0\rangle + \sin(\Omega t/2)|1\rangle. \tag{3}$$

In a quantum Zeno system, however, spontaneous emission is introduced, coupling the system to a reservoir. Standard quantum treatment of such systems is via a master equation for the system density matrix. In the current model, the scattered state after a spontaneous decay corresponds to the photon escaping from the system. Due to irreversibility, this state is dynamically decoupled from the rest of the system during the subsequent evolution of the system. This allows us to map the master equation onto a pure-state representation, in which the system state is represented by a pure state in the unscattered subspace. The master equation dynamics can be then be exactly reproduced if this pure state evolves under an effective non-Hermitian Hamiltonian. Because of the non-Hermitian property, the state in this representation will no longer be normalized to unity as time evolves. This loss of normalization corresponds to the probability that the system has decayed. After a successful Zeno-gate operation, however, the system decay is prohibited by the Zeno effect. The quantum state of the system is then the evolved pure state, which must be renormalized to unity.

For the system depicted in Fig. 1, the state $|1\rangle$ decays at rate Γ to a third state $|g\rangle$. The effective non-Hermitian Hamiltonian in the pure-state representation of $\{|0\rangle, |1\rangle\}$ is then

$$\hat{H}_{\text{eff}} = \hat{H}_\Omega - i\frac{\hbar\Gamma}{2}|1\rangle\langle 1|. \tag{4}$$

The derivation of this effective Hamiltonian, as well as further explanations of the pure-state representation, is given in Appendix A. The reduction in normalization, $P(t) = \langle\Psi(t)|\Psi(t)\rangle$, corresponds to the probability that the system has decayed to state $|g\rangle$.

This evolution can be solved analytically, and in the regime $\Gamma \gg \Omega$, we find that the probability for the system to be found in the initial state $|0\rangle$ is given by $P_0(t) = e^{-\Omega^2 t/\Gamma}$. In the relevant case $\Omega t \sim 1$ and $\Gamma t \gg 1$, this becomes

$$P_0(t) \approx 1 - \frac{(\Omega t/2)^2}{\Gamma t/4}, \tag{5}$$

which approaches unity as Γt is increased with Ωt held fixed, in which limit the system is again frozen in the initial state. The discrete and continuous systems can be mapped onto one another if we equate $\theta \leftrightarrow \Omega t/2$ and $M \leftrightarrow M_{\text{eff}} = \Gamma t/4 = \theta\Gamma/2\Omega$. The equivalence between the two systems can be understood by interpreting the spontaneous emission in the continuous case as a source of effective "measurements" by the reservoir. The measurements are implemented because the presence or absence of spontaneously emitted photons will immediately reveal the state information and collapse the system into either $|1\rangle$ or $|0\rangle$. For a decay rate Γ, a single effective measurement duration is $4\Gamma^{-1}$. The effective number of measurements M_{eff} during an interval t is therefore $t/4\Gamma^{-1} = \Gamma t/4$. Equations (5) and (1) are in this sense exactly equivalent. We note that a large M_{eff} corresponds to a large ratio of Γ/Ω, and hence a stronger dissipation is favorable for the continuous system. This is exactly opposed to the conventional approach, where dissipation must be negligible during a quantum gate operation.

Using these results for the quantum Zeno effects, we now describe the general theory of quantum Zeno gates. Our model applies to both the discrete and continuous Zeno effects, as they can be exactly mapped onto each other. We will therefore treat only the continuous Zeno effect, with the understanding that analogous results for the discrete Zeno effect can be obtained by substituting M for M_{eff}. We show the generalized two-qubit logic gates can be realized via a single IFM in a direct or indirect manner. For the direct gate, one qubit acts as a "probe," probing the quantum state of the "object" qubit repeatedly or continuously, while the object qubit is coherently driven on a time scale slow compared to the measurement time. The coherent evolution of the probe qubit will be allowed or prohibited depending on the state of the object qubit and thus will create entanglement to implement the gate operation. This gate, however, requires the two qubits to start inside the DFS, as states outside the DFS will immediately decay, resulting in loss of quantum information. Such direct gates are therefore incapable of implementing unitary operations, which must be defined for all possible input states. We have found that with the addition of an ancillary qubit unitary quantum phase gates can be realized, even without the need to measure the final state of the ancillary qubit. In these gates, the ancillary qubit acts as the probe measuring the joint quantum state of the two logical qubits, while the three qubits remain in a DFS.

For the direct logic gate, only two qubits are involved. As shown in Fig. 2, only the $|00\rangle$ state decays, so that the $|01\rangle$, $|10\rangle$, and $|11\rangle$ states form a DFS, where the two-qubit states are in the form $|q_1 q_2\rangle$, with q_1 and q_2 the probe and object qubits, respectively. Achieving this state-selective decoherence is the primary design challenge in physical implementation of such gates. We will see, however, that the DFS states correspond to states with no interaction between them, i.e., their wave function overlap is zero.

As the two logical qubits are required to be initially in the DFS, their initial state is

$$|\Psi_i\rangle = c_{01}|01\rangle + c_{10}|10\rangle + c_{11}|11\rangle. \tag{6}$$

The coefficients c_{ij}, with $i, j = 0, 1$, are arbitrary and normalized to 1. The goal is to transform this state to the final state
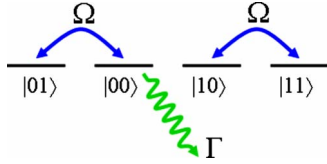
FIG. 2. (Color online) Scheme for the direct two-qubit quantum Zeno gate via a single IFM. Each state is of the form $|q_1q_2\rangle$, where q_1 and q_2 are the probe and object qubits. The coherent Rabi oscillation is applied to the probe qubit as indicated by the blue arrows, while the green arrow indicates spontaneous decay.

$$|\Psi_f\rangle = c_{01}|01\rangle + (c_{10}\cos\theta - c_{11}\sin\theta)|10\rangle$$
$$+ (c_{10}\sin\theta + c_{11}\cos\theta)|11\rangle, \qquad (7)$$

with θ arbitrarily adjustable. Applying a slow σ_y pulse to the probe qubit rotates its state according to Hamiltonian (2). The attempt to rotate the probe qubit will therefore take the system out of the DFS if the object qubit is in the state $|0\rangle$, in which case the quantum Zeno effect will freeze the system in its initial state and prevent the rotation of the probe qubit. Only if the object qubit is in the $|1\rangle$ state will the ancillary qubit undergo rotation and change its state. The final state of the system will then be (7) with $\theta = \Omega t/2$, and thus the desired target state is obtained. The success probability in this gate operation is given by the standard Zeno formula

$$P_{\text{success}} = 1 - |c_{01}|^2 \frac{\theta^2}{M_{\text{eff}}}, \qquad (8)$$

where the effective number of measurements is $M_{eff} = \theta\Gamma/2\Omega$.

We now describe a quantum Zeno phase gate based on a three-qubit system, where one qubit serves as an ancillary, and two are the logical qubits. The operation of a phase gate on a two-qubit state is to transform an initial state of

$$|\Psi_i\rangle = c_{00}|00\rangle + c_{01}|01\rangle + c_{10}|10\rangle + c_{11}|11\rangle \qquad (9)$$

into the final state

$$|\Psi_f\rangle = c_{00}|00\rangle + c_{01}|01\rangle + c_{10}|10\rangle - c_{11}|11\rangle. \qquad (10)$$

Our scheme consists of a pair of logical qubits in an arbitrary initial state, together with a third ancillary qubit prepared in the $|0\rangle$ state. The initial state of the system is therefore

$$|\Psi_{in}\rangle = c_{00}|000\rangle + c_{01}|010\rangle + c_{10}|100\rangle + c_{11}|110\rangle, \quad (11)$$

where the three-qubit states are in the form $|q_1q_2a\rangle$, with q_1 and q_2 the logical qubit quantum numbers and a describing the ancillary qubit. A single-qubit 2π pulse is applied to the ancillary qubit, rotating its state from $|0\rangle$ through $|1\rangle$ and back to $-|0\rangle$, which imprints a π phase shift on the state of the system in the absence of dissipation. The complete state space of the three-qubit system consists of eight states. As shown in Fig. 3, the states $|000\rangle$, $|100\rangle$, $|010\rangle$, $|110\rangle$, and $|111\rangle$ form a DFS, while the states $|001\rangle$, $|101\rangle$, and $|011\rangle$ decay at rates 2Γ, Γ and Γ, respectively. The decay rate for state $|001\rangle$ is doubled because there exist two possible decay channels, i.e., of q_1,a and q_2,a. The attempt to rotate the ancillary qubit will therefore take the system out of the DFS
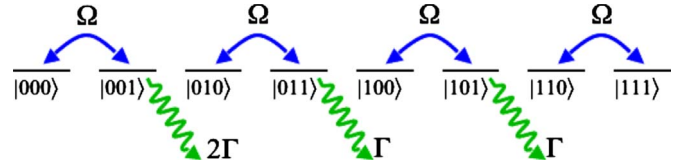
FIG. 3. (Color online) Scheme for a two-qubit phase gate with an ancillary qubit. Each state is of the form $|q_1q_2a\rangle$, where q_1 and q_2 are the logical qubits and a is the ancillary qubit. Note that the coherent Rabi coupling, indicated by the blue arrows, is applied to the ancillary qubit.

if the logical qubits are in the states $|00\rangle$, $|01\rangle$, or $|10\rangle$, in which case the Zeno effect will prohibit the rotation. The ancillary qubit will thus undergo rotation only if the logical qubits are in the $|11\rangle$ state, after which the π phase shift is imprinted. The final state of the system will thus be

$$|\Psi_{\text{out}}\rangle = (c_{00}|00\rangle + c_{01}|01\rangle + c_{10}|10\rangle - c_{11}|11\rangle) \otimes |0\rangle_a \qquad (12)$$

with probability

$$P_{\text{success}} = 1 - \left(\frac{|c_{00}|^2}{2} + |c_{01}|^2 + |c_{10}|^2\right)\frac{\pi^2}{M_{\text{eff}}}. \qquad (13)$$

Here $M_{\text{eff}} = \pi\Gamma/2\Omega$. The extra factor of $\frac{1}{2}$ for the $|00\rangle$ state is because the relevant decay rate is then 2Γ, resulting in a doubled number of effective measurements. Upon successful operation, the phase gate has been applied and the state of the ancillary qubit is not entangled with that of the logical qubits, so that no measurement of the ancillary qubit and/or conditional operations are required.

Lastly, we note that for both the direct and indirect quantum Zeno gates successful operation indicates that the system remained in the DFS throughout, so that entanglement has been achieved without any interaction between qubits. Merely the possibility of dissipative interaction and the constant monitoring of the system by its environment are sufficient to project the system into an entangled state. As fast gate operation at high success probability is desired for scalable quantum computation, one should seek out a system with as large a decay rate Γ as possible, which is exactly the opposite regime one normally attempts to reach when quantum logic gates are based on ordinary coherent qubit-qubit interactions.

III. ELEMENTARY ATOM-PHOTON QUANTUM ZENO GATES

Now we consider physical implementations of quantum Zeno logic gates based on a single photon propagating in a high-finesse ring cavity which interacts with a single atom. The quantum logic circuits we propose are built from two elementary interaction-free quantum gates, which we term the interaction-free polarization gate (IFPG) and the interaction-free Raman gate (IFRG). The IFPG is a generalization and refinement of previously proposed interaction-free gates [50,51], and induces a rotation in the polarization of a photon conditioned on the state of a control atom. The IFRG
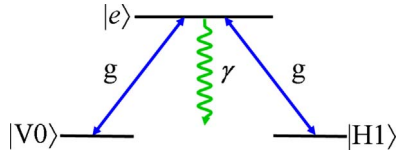
FIG. 4. (Color online) Level scheme for the elementary IFPG and IFRG gates. The states $|V0\rangle$ and $|H1\rangle$ are resonantly coupled to the excited state $|e\rangle$ with coupling strength g, while the state $|e\rangle$ spontaneously decays at rate γ.

reverses the roles of atom and photon and induces a rotation of the atomic hyperfine state conditioned on the polarization of a control photon. The atom-photon interaction in these gates is based on a standard Λ-level scheme. The two atomic ground hyperfine states are labeled $|0\rangle$ and $|1\rangle$, and are coupled to an excited state $|e\rangle$ via absorption or emission of cavity photons with two orthogonal polarizations, labeled $|V\rangle$ and $|H\rangle$, respectively. We note that this choice of labels is purely symbolic, and in practice the two states will most likely be circular polarization states. The use of H and V is, however, in keeping with the early literature on interaction-free quantum interrogation [42,45]. For the case of a single photon in the ring cavity, the joint photon-atom states $|V0\rangle$ and $|H1\rangle$ couple strongly to $|e\rangle$, which then decays via spontaneous emission to a set of states having zero photons in the cavity, as shown in Fig. 4. Due to selection rules, the joint states $|H0\rangle$ and $|V1\rangle$ are not coupled to $|e\rangle$. Quantum back reaction due to the nonemission of a photon therefore collapses the joint state onto the $\{|V1\rangle|H0\rangle\}$ subspace. For simplicity, we temporarily assume that the states $|H0\rangle$ and $|V1\rangle$ will immediately decay with unit probability.

The interaction-free polarization gate is shown in Fig. 5(a), with Fig. 5(b) depicting a graphical representation of the gate. The circuit is modeled after the standard high-efficiency quantum interrogation circuit [42], which we have generalized to allow an arbitrary polarization rotation angle θ, rather than the standard $\pi/2$ rotation. The gate consists of
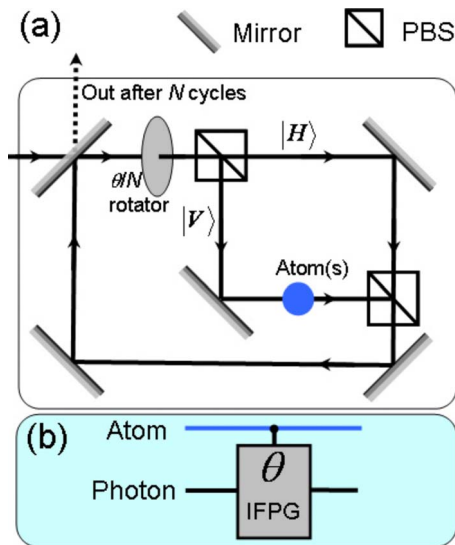
FIG. 5. (Color online) (a) Schematic illustration of the physical implementation of the IFPG; (b) its graphic representation.
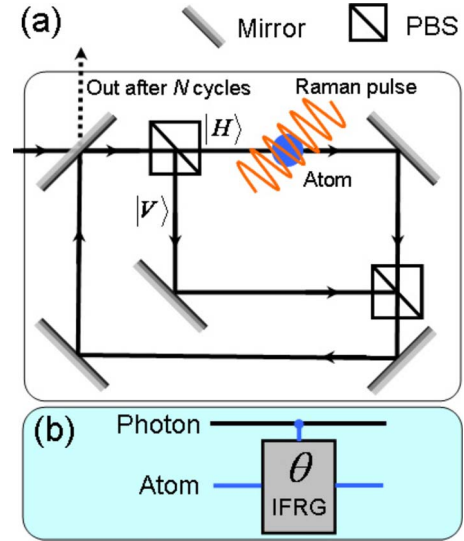
FIG. 6. (Color online) (a) Schematic illustration of the physical implementation of the IFRG; (b) its graphic representation.

a high-finesse optical ring resonator, into which a single photon is injected and then released after N cycles. Each cycle consists of passage through a θ/N polarization rotator followed by a pair of polarized beam splitters (PBSs), which spatially separate the H and V polarizations. The control atom is placed in the V arm. The input state must be of the form

$$|\Psi_{in}\rangle = c_{H0}|H0\rangle + c_{H1}|H1\rangle + c_{V1}|V1\rangle, \qquad (14)$$

as the $|V0\rangle$ state leads to immediate loss of the photon via spontaneous emission. As only the V polarization interrogates the atom, it follows that the atomic state $|1\rangle$ is transparent to the photon. In this case, the effect of the atom is negligible, and the photon polarization rotates by the angle θ. If the atom is in state $|0\rangle$, however, the quantum Zeno effect will freeze the photon in the $|H\rangle$ state. Assuming successful operation, this leads to the output state

$$|\Psi_{out}\rangle = c_{H0}|H0\rangle + (c_{H1}\cos\theta - c_{V1}\sin\theta)|H1\rangle$$
$$+ (c_{H1}\sin\theta + c_{V1}\cos\theta)|V1\rangle, \qquad (15)$$

which shows that the photon polarization is rotated conditioned on the atom being in state $|1\rangle$.

The complementary interaction-free Raman gate is depicted in Figs. 6(a) and 6(b). It differs from the IFPG in that the atom is placed in the H arm, and the polarization rotator is replaced by a Raman pulse which couples the $|0\rangle$ and $|1\rangle$ atomic states via a $\hat{\sigma}_y$ rotation. The $\hat{\sigma}_y$ operation is timed so that the atomic state rotates by angle θ during the time it takes for the photon to travel N ring-cavity cycles. An arbitrary input state is of the form

$$|\Psi_{in}\rangle = c_{H0}|H0\rangle + c_{V0}|V0\rangle + c_{V1}|V1\rangle, \qquad (16)$$

where the state $|H1\rangle$ is forbidden. If the photon is in $|H\rangle$, the quantum Zeno effect freezes the atom in the $|0\rangle$ state; otherwise, the atomic spin rotates by θ. Upon successful operation, this results in the output state
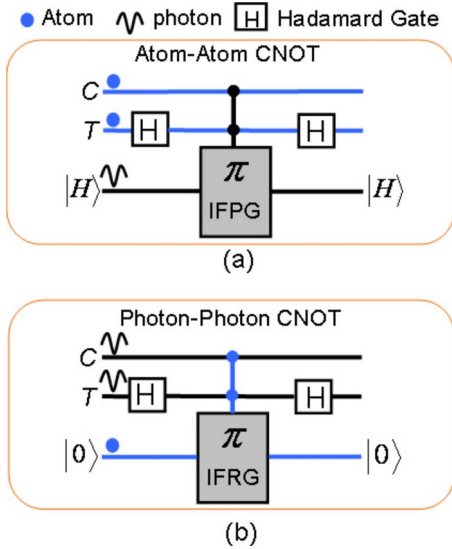
FIG. 7. (Color online) Graphical logic circuits for atom-atom (a) and photon-photon (b) CNOT gate. In both figures, we use C for the control and T for the target qubit.

$$|\Psi_{\text{out}}\rangle = c_{H0}|H0\rangle + (c_{V0}\cos\theta - c_{V1}\sin\theta)|V0\rangle + (c_{V0}\sin\theta + c_{V1}\cos\theta)|V1\rangle, \quad (17)$$

which shows that the atomic state is rotated conditioned on the photon being in state $|V\rangle$.

IV. QUANTUM ZENO CNOT GATES

From these two elementary gates, we can construct the primary quantum logic gates necessary for universal quantum computation. The first gate we consider is the atom-atom controlled-NOT gate, depicted schematically in Fig. 7(a). In a CNOT gate, the state of the target qubit is flipped if the control qubit is in the logical $|1\rangle$ state, and is left unchanged otherwise. Our atom-atom CNOT gate uses a single IFPG with $\theta = \pi$, but with *two* atoms placed in the $|V\rangle$ arm. One atom serves as the control qubit and the other serves as the target. A single ancillary $|H\rangle$ photon is injected into the device to induce atom-atom entanglement via noninteraction with both atoms. The control atom differs from the target in that Hadamard transformations are applied to it before and after the interaction with the photon. For the IFPG with two atoms and one photon, the initial state is

$$|\Psi_{\text{in}}\rangle = |H\rangle \otimes (c_{00}|00\rangle + c_{01}|01\rangle + c_{10}|10\rangle + c_{11}|11\rangle). \quad (18)$$

If either atom is in the state $|0\rangle$, it will be sufficient to induce the quantum Zeno effect and freeze the photon in the $|H\rangle$ state. Thus only the $|11\rangle$ state is transparent to the photon, in which case the photon undergoes a π rotation $|H\rangle \to -|H\rangle$. The output state of the two-atom π IFPG is then

$$|\Psi_{\text{out}}\rangle = |H\rangle \otimes (c_{00}|00\rangle + c_{01}|01\rangle + c_{10}|10\rangle - c_{11}|11\rangle), \quad (19)$$

thus realizing a two-atom *phase gate*. It is known that a phase gate can be transformed into a CNOT gate via single-qubit operations, such as the Hadamard transform, defined as
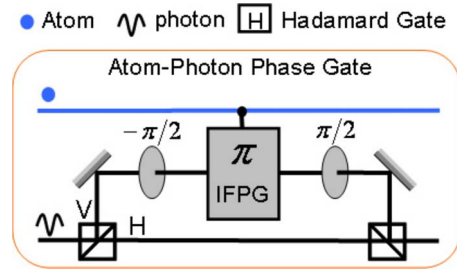
FIG. 8. (Color online) Graphical logic circuits for the atom-photon phase gate.

$|0\rangle \to (|0\rangle + |1\rangle)/\sqrt{2}$ and $|1\rangle \to (|0\rangle - |1\rangle)/\sqrt{2}$. Applying this transform to the state of the target atoms before and after the action of the π IFPG gives the output state

$$|\Psi_{\text{out}}\rangle = |H\rangle \otimes (c_{00}|00\rangle + c_{01}|01\rangle + c_{11}|10\rangle + c_{10}|11\rangle), \quad (20)$$

corresponding to a CNOT operation on the two atoms. Due to our use of a π polarization rotation, as opposed to the $\pi/2$ rotation of the standard IFM circuit, we find that at the output the photon is not entangled with the atoms. Because of this disentanglement, no detection of the photon and/or its polarization state is necessary. We note that during the N cycles of the IFPG, the atoms and photon move through a highly entangled three-body state.

A photon-photon CNOT gate can be constructed similarly by injecting two photons into a π IFRG containing a single ancillary atom. In this case, the control and target photons can be input as time-separated wave packets, or counter-propagate in the ring cavity. This gate is depicted schematically in Fig. 7(b). The analysis is the same as for the atom-atom CNOT gate, with $H \leftrightarrow 0$ and $V \leftrightarrow 1$. After successful operation, the state of the atom is not entangled with the two-photon state, so that no atomic-state measurement is required for successful photon-photon gate operation.

A hybrid atom-photon CNOT gate, in which a stationary atomic qubit and a flying photonic qubit play the roles of control and target, can be constructed without the use of a third ancillary particle. In Fig. 8, we depict an atom-photon phase gate. The input state for this gate is

$$|\Psi_{\text{in}}\rangle = c_{H0}|H0\rangle + c_{H1}|H1\rangle + c_{V0}|V0\rangle + c_{V1}|V1\rangle. \quad (21)$$

The first PBS sends the $|V\rangle$ polarization state along an upper arm, where a $-\pi/2$ rotator converts it to $|H\rangle$ polarization. The state of the system is then

$$|\Psi\rangle = c_{H0}|H0\rangle + c_{H1}|H1\rangle + c_{V0}|H'0\rangle + c_{V1}|H'1\rangle, \quad (22)$$

where the prime indicates the upper path. The π IFPG then transforms the system to the state

$$|\Psi\rangle = c_{H0}|H0\rangle + c_{H1}|H1\rangle + c_{V0}|H'0\rangle - c_{V1}|H'0\rangle. \quad (23)$$

The subsequent $-\pi/2$ rotation on the upper arm and the PBS restores the $|H'\rangle$ state to $|V\rangle$, resulting in the desired phase-gate output state

$$|\Psi_{\text{out}}\rangle = c_{H0}|H0\rangle + c_{H1}|H1\rangle + c_{V0}|V0\rangle - c_{V1}|V1\rangle. \quad (24)$$
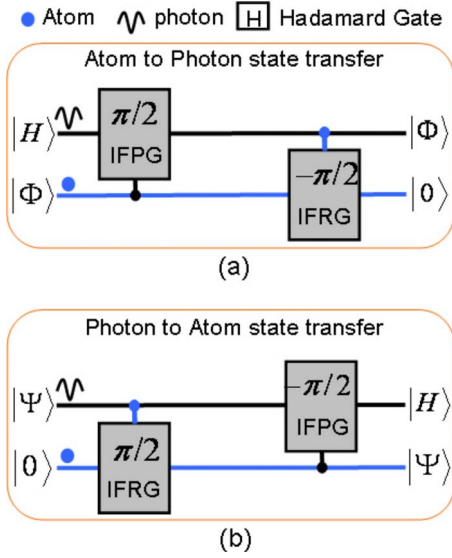
FIG. 9. (Color online) Graphical state transfer circuits for atom to photon (a) and photon to atom (b), where $|\Phi\rangle$ and $|\Psi\rangle$ denote the arbitrary atomic and photonic states, respectively.

This state can then be converted into a CNOT gate by the addition of single-qubit Hadamard transformations onto the target qubit before and after the operation of the phase gate. Thus either the atom or the photon can play the role of control qubit simply by application of the Hadamard sequence to the other particle.

Lastly, we note that Azuma [51,52] recently proposed an alternative CNOT gate using essentially three IFM gates to prepare the required ancillary qubits, at least two more IFM gates for the required two Bell measurements, as well as a considerable number of single-qubit measurements and measurement-conditioned operations. Thus we believe that our gates represent a significant advance, as they are accomplished within only a single IFM device and two logical Hadamard or rotation operations, and, most importantly, without any measurements or conditional operations.

V. STATE TRANSFER CIRCUITS

We now turn our attention to state transfer circuits, which map the quantum state of an atom onto a photon and vice versa. Unlike the CNOT gates, state transfer circuits require two elementary interaction-free quantum Zeno gates. The first serves to entangle the atom and photon, while the second is required for disentanglement. The atom-to-photon state transfer circuit is depicted in Fig. 9(a). It consists of a $\pi/2$ IFPG followed by a $-\pi/2$ IFRG. The photon is prepared in the $|H\rangle$ state, and the atom is initially in the unknown quantum state $c_0|0\rangle + c_1|1\rangle$. The goal of the circuit is then to transfer this unknown quantum state onto the state of the photon. With the input state taken as

$$|\Psi_{\text{in}}\rangle = |H\rangle \otimes (c_0|0\rangle + c_1|1\rangle) = c_0|H0\rangle + c_1|H1\rangle, \quad (25)$$

the action of the $\pi/2$ IFPG is to rotate the polarization of the photon by $\pi/2$ conditioned on the atom being in state $|1\rangle$, resulting in the state

$$|\Psi\rangle = c_0|H0\rangle + c_1|V1\rangle. \quad (26)$$

The $-\pi/2$ IFRG rotates the atomic state by $-\pi/2$ conditioned on the photon being in state $|V\rangle$, resulting in the output state

$$|\Psi_{\text{out}}\rangle = c_0|H0\rangle + c_1|V0\rangle = (c_0|H\rangle + c_1|V\rangle) \otimes |0\rangle. \quad (27)$$

Thus the quantum state of the atom is written onto the photon, and the atom and photon are successfully disentangled. The reverse photon-to-atom state transfer circuit is depicted in Fig. 9(b). It operates identically to the atom-to-photon circuit, except that the roles of atomic and photonic qubits are reversed. We emphasize here that the present state transfer gates operate without the need to measure the final state of the particle initially possessing the unknown state. This is clearly different and significantly improved from several previously studied schemes, where a final (Bell) measurement is required [1,12,23,24,56–60]. We note that a measurement-free state mapping scheme between a coherent light field in a high-finesse optical cavity and a single atom has been recently demonstrated [29].

VI. EXTENSION: LONG-DISTANCE QUANTUM COMMUNICATION

In above discussions, we have constructed the atom-atom phase (CNOT) gate using a single IFM device, where the two atomic qubits are required to be in a common optical resonator. This requirement restricts such a circuit to two qubits separated within one resonator length. For the purpose of quantum communications and/or gate operations between two distant atomic qubits, one alternative approach would be to indirectly entangle them via mutual noninteraction with a common ancillary photon.

As a first example, we deviate from the measurement-free feature and show that two uncorrelated qubits can be collapsed to the Bell $\Phi^{\pm}$ or $\Psi^{\pm}$ subspaces by using two atom-photon Zeno CNOT gates and measuring the final photon state. We note that for quantum communication via a lossy photonic channel, verifying the presence of the transported photon is somewhat helpful as it can detect the photon loss and thus improve the operation fidelity upon heralded success. In our scheme, the photon is initially in the $|H\rangle$ state and the two atoms are in arbitrary states. The initial state of the system is then written as

$$|\Psi_{\text{in}}\rangle = |H\rangle \otimes (c_{00}|00\rangle + c_{01}|01\rangle + c_{10}|10\rangle + c_{11}|11\rangle). \quad (28)$$

The photon noninteracts with the first atom via the atom-photon Zeno CNOT gate, where its polarization reverses $(|H\rangle \leftrightarrow |V\rangle)$ only if the atomic qubit is in state $|1\rangle$. The system afterwards will be in

$$|\Psi'\rangle = |H\rangle \otimes (c_{00}|00\rangle + c_{01}|01\rangle) + |V\rangle \otimes (c_{10}|10\rangle + c_{11}|11\rangle). \quad (29)$$

After transmission, the photon then noninteracts with the second atom via a second identical Zeno CNOT gate, transforming the system into
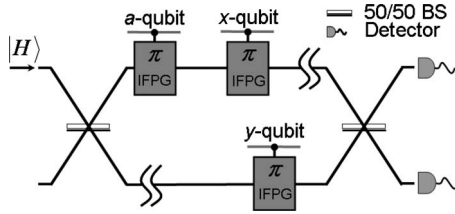
FIG. 10. Schematic setup for long-distance entanglement generation with built-in error correction. A photon in $|H\rangle$ polarization state is passed through a MZ interferometer with three π IFPGs, and is then measured by two detectors placed at the two interferometer outputs. The MZ interferometer consists of two 50:50 linear beam splitters (BSs) with a $\pi/2$ phase imprinted on the reflected photons. In figure, we label the ancillary and the two logical qubits as a, x, and y qubits, respectively.

$$|\Psi_{\text{out}}\rangle = |H\rangle \otimes (c_{00}|00\rangle + c_{11}|11\rangle) + |V\rangle \otimes (c_{10}|10\rangle + c_{01}|01\rangle). \tag{30}$$

Accomplishing the quantum communication then requires measuring the photon on the H-V basis. If it is measured in $|H\rangle$, the two atoms will be collapsed onto $c_{00}|00\rangle + c_{11}|11\rangle$ state, or the $\Phi^\pm$ subspace. Otherwise, they will be collapsed to the $c_{01}|01\rangle + c_{10}|10\rangle$ state, or the $\Psi^\pm$ subspace. In either way, entanglement between the two is established, based on which long-distance logic gates can be realized with the addition of single-qubit operations.

A main and common difficulty in quantum communication between distant qubits is photon loss during transmission, where the loss probability increases exponentially with the transport distance. In schemes based on cavity QED [19–22], the quantum states of atomic qubits are encoded in the internal (polarization) states of photons. A lost photon will therefore immediately collapse the atomic state(s) and destroy the qubit(s) via decoherence. This problem also exists in the above scheme, where the intermediate photon state is $|H\rangle$ or $|V\rangle$ depending on the first qubit being in $|0\rangle$ or $|1\rangle$, as shown in (29). One possible way to overcome this difficulty is to combine the atom-photon phase gate with interferometric phase measurements, as a photon lost inside an interferometer does not reveal the quantum state of the measured qubits [27]. In the following we neglect detector inefficiency and dark-count rates at present, to focus on the problem of transmission loss.

As an example, here we describe a photon-loss-tolerant protocol using π IFPGs and a Mach-Zehnder (MZ) interferometer. The schematic setup is depicted in Fig. 10, where we introduce an ancillary qubit (a qubit) to restore the quantum states of the two logical qubits in the case of photon loss. In the scheme, a photon in $|H\rangle$ state is passed through a 50:50 beam splitter and then guided through the π IFPG gates where it noninteracts successively with the ancillary and x atom in the upper arm, or the y atom in the lower arm. The initial state of the system is

$$|\Psi_{\text{in}}\rangle = |H\rangle \otimes |\Psi\rangle_a \otimes (c_{00}|00\rangle + c_{01}|01\rangle + c_{10}|10\rangle + c_{11}|11\rangle), \tag{31}$$

with the ancillary atom prepared in the state

$$|\Psi\rangle_a = \frac{1}{\sqrt{2}}(|0\rangle_a + |1\rangle_a). \tag{32}$$

After the photon passes through the first beam splitter and noninteracts with the ancillary and the first logical qubit (x qubit) via π IFPG gates, the system will be in the state

$$\begin{aligned} |\Psi'\rangle = \frac{1}{2}[&|H\rangle_u \otimes (|0\rangle_a - |1\rangle_a) \otimes (c_{00}|00\rangle - c_{01}|01\rangle + c_{10}|10\rangle \\ &- c_{11}|11\rangle) + i|H\rangle_l \otimes (|0\rangle_a + |1\rangle_a) \otimes (c_{00}|00\rangle + c_{01}|01\rangle \\ &+ c_{10}|10\rangle + c_{11}|11\rangle)], \end{aligned} \tag{33}$$

where $|H\rangle_{u,l}$ indicates the photon in the upper and lower interferometer arms. In the absence of photon loss, the final state, obtained after the photon noninteracts with the second qubit (y qubit) via another identical π IFPG and then passes the second beam splitter, is

$$\begin{aligned} |\Psi_{\text{out}}\rangle = &(|H\rangle_u|0\rangle_a - i|H\rangle_l|1\rangle_a) \otimes (c_{01}|01\rangle - c_{10}|10\rangle) \\ &- (|H\rangle_u|1\rangle_a - i|H\rangle_l|0\rangle_a) \otimes (c_{00}|00\rangle - c_{11}|11\rangle). \end{aligned} \tag{34}$$

Measuring both the final states of the photon and the ancillary atom will thus project the two atoms onto either the $c_{01}|01\rangle - c_{10}|10\rangle$ or the $c_{00}|00\rangle - c_{11}|11\rangle$ state, which establishes the desired entanglement. Otherwise, if neither of the photon detectors is triggered, it is most likely that the photon is lost during transmission from either of the interferometer arms, but without knowing from which. Assuming equal loss possibilities for the two arms, the system will now be in a statistical mixture of

$$\rho^{\text{loss}} = \langle H|_u \Psi'\rangle\langle\Psi'|H\rangle_u + \langle H|_l \Psi'\rangle\langle\Psi'|H\rangle_l. \tag{35}$$

We then need to measure the ancillary atom on the $|\pm\rangle_a = (|0\rangle_a \pm |1\rangle_a)/\sqrt{2}$ basis, and restore the quantum states of the qubits according to the measurement result. If it is measured in $|+\rangle$, the state of two atomic qubits is automatically restored, as seen in (33). Otherwise, if it is measured in $|-\rangle$, the atoms will be in the state

$$c_{00}|00\rangle - c_{01}|01\rangle + c_{10}|10\rangle - c_{11}|11\rangle, \tag{36}$$

and a relative π phase applied on the first qubit immediately recovers the original quantum state of the two qubits. Upon recovery, the whole procedure can be repeated, until success.

VII. SUCCESS PROBABILITY

In describing each of these quantum Zeno circuits, we have assumed successful operation, and shown that the desired output could be achieved. In actuality, the descriptions we have provided are only exact in the limit $N \to \infty$, where N is the number of times the photon cycles through the ring cavity. Three key factors determine the success probability. The first is finite N, restricted primarily by the reflectivity of the cavity mirrors and imperfections in whatever optical elements are included in the circuit. The second effect is imperfect absorption of the $|V0\rangle$ state, which we characterize by the parameter ϵ_0, so that the absorption probability for this

state is $1 - \epsilon_0$. Due to this imperfection, the effective number of measurements for N feedback cycles is reduced to $(1 - \epsilon_0)N$. The third factor is imperfect transparency of the $|V1\rangle$ state, characterized by the absorption probability ϵ_1. For an ideal system we would have $\epsilon_0 = \epsilon_1 = 0$, indicating that the selection rules of Fig. 4 are precisely obeyed. In practice we expect finite selection-rule errors due to the combined effects of tight focusing of the photon, which warps the photon polarization vector; and tight trapping of the atom, which may warp the atomic hyperfine spin vector. We use the term "warp" to indicate an undesired spatial dependence. A rigorous calculation of these errors will be investigated in future work. At present we calculate only the effects of nonzero ϵ_0 and ϵ_1 and determine the acceptable upper limits on these two parameters.

As was shown in Sec. II, a quantum Zeno system, while being an open system, can nonetheless be described in the pure-state representation, governed by a non-Hermitian Hamiltonian. For the single-atom IFPG, the quantum state of the system can be represented by a pure state in the $\{|H0\rangle, |H1\rangle, |V0\rangle, |V1\rangle\}$ subspace. The final state can be derived from the initial state via a nonunitary propagator $|\Psi_{\text{out}}\rangle = \hat{V}(\theta, N, \epsilon_0, \epsilon_1)|\Psi_{\text{in}}\rangle$, and the decay probability determined by $P_{\text{decay}} = 1 - \langle\Psi_{\text{out}}|\Psi_{\text{out}}\rangle$. The exact form of the propagator $\hat{V}(\theta, N, \epsilon_0, \epsilon_1)$ is derived in Appendix A [Eq. (B7)]. The overall success probability, which is the probability for the system to be found in the target state at the output, is given by $P_{\text{success}} = |\langle\Psi_{\text{target}}|\Psi_{\text{out}}\rangle|^2$. Note that, since $|\Psi_{\text{out}}\rangle$ is now not normalized to unity, P_{success} has implicitly taken into account the decay possibility.

If we consider the π IFPG with an input state of the form (14) we find that the decay probability is given by

$$P_{\text{decay}} = |c_{H0}|^2 \lambda_0 + (|c_{H1}|^2 + |c_{V1}|^2)\lambda_1, \qquad (37)$$

where

$$\lambda_0 = \frac{\pi^2}{N} \frac{1 + \sqrt{\epsilon_0}}{1 - \sqrt{\epsilon_0}} - \frac{\pi^2}{N^2}\epsilon_0 \qquad (38)$$

and

$$\lambda_1 = 1 - e^{-\epsilon_1 N/2} - \left(\frac{N\epsilon_1}{10}\right)^4. \qquad (39)$$

The quantum gate can be considered "efficient" if the failure probability scales as $P_{\text{decay}} \sim \frac{1}{N}$, which therefore requires $1 - \sqrt{\epsilon_0} \sim 1$ and $\epsilon_1 \sim \frac{1}{N^2}$. The overall success probability is given to leading order by

$$P_{\text{success}} = 1 - P_{\text{decay}} + O\left(\frac{1}{N^2}\right) = 1 - O\left(\frac{1}{N}\right), \qquad (40)$$

characteristic of high-efficiency quantum interrogation. We note that the IFRG operates on the same principles, and thus exhibits the same $1/N$ scaling behavior.

The condition $1 - \sqrt{\epsilon_0} \sim 1$ indicates that ϵ_0 need not be negligible, but rather only not too close to 1. This requirement is not very stringent, as previously described by Azuma [51]. We note, however, that previous authors have not considered imperfect transparency of the $|V1\rangle$, described by ϵ_1.

We see that this is actually the critical parameter upon which successful operation is sensitively dependent. For an N of 10^3, Eq. (39) implies that the absorption probability should be $\sim 10^{-6}$ in order to maintain $1/N$ scaling. Clearly this will require very precise control over the atom-photon interaction. At present we do not know if it is possible to maintain both of these error parameters in their operational ranges simultaneously, although the weak constraint on ϵ_0 leads us to be optimistic. In future research we will address the interaction between tightly trapped atoms and tightly focused photons in detail.

If we assume that absorption in the transparent state is negligible, the absorption of the absorbing state can be estimated using the standard cross section of a two-level atom scattering resonant light, $\sigma = \lambda^2/2$. The absorption probability is thus determined by the ratio of σ to the focusing area A of the photon. Assuming a tightly focused light beam with transverse radius W, the absorption probability is thus

$$1 - \epsilon_0 = \frac{1}{2\pi}\left(\frac{\lambda}{W}\right)^2. \qquad (41)$$

Taking the diffraction limit $W = \lambda$ gives

$$\lambda_0 \approx \frac{250}{N}. \qquad (42)$$

This means that for $N = 10^3$ the imperfection in absorption degrades the success probability from $\sim 99\%$ to $\sim 75\%$, and for $N = 10^4$ from 99.9% to 97.5%. On the other hand, to compensate for this small absorption probability would require an increase in the cycle parameter N by a factor of 25.

We can relate the maximum achievable cycling parameter N to the cavity finesse by taking into account the round-trip net transmission probability T. The probability to survive N cavity round trips is R^N, where $R = 1 - T$. Thus the total loss probability due to imperfect optics is $P_{\text{loss}} = 1 - R^N = 1 - (1 - T)^N \approx NT$. In order to maintain the $250/N$ success rate imposed by a realistic absorption probability, this requires $T \sim 250/N^2$, in analogy with the imperfect atomic transparency parameter ϵ_1. Presently, high-finesse supermirrors [28,29] can have $T < 10^{-6}$, which would correspond to $N \sim 1.5 \times 10^4$. An N of this size permits an overall success probability for the quantum Zeno gates of 98.4%, which would be competitive against potential competing methods. At present, achieving a net round-trip transmission probability of 10^{-6} for a single-photon pulse, while perhaps conceivable, would clearly require heroic experimental efforts.

Lastly, we note that for conventional schemes based on cavity QED, the system is operated in the strong-coupling regime, where vacuum Rabi oscillations dominate the dissipative atomic decay and cavity leakage [28,29,61]. This regime is characterized by a large single-atom cooperativity parameter, e.g., $C = g_c^2/\Gamma_c\kappa_c \gg 1$, where g_c, Γ_c, and κ_c represent the atom-cavity coupling strength, the atomic spontaneous emission rate inside the cavity, and the cavity decay rate, respectively. Unlike the cavity QED gates, the present Zeno gates are implemented in ring cavities. The coupling strength and spontaneous emission rate in these systems are given by

their free-space values g and Γ. The mean lifetime of photons inside the ring cavity is $\tau \simeq L/cT$, corresponding to a cavity decay rate of $\kappa = 1/\tau = cT/L$. Here c is the speed of light, and L is the path length of a single round trip through the ring cavity, which we shall take as the coherent length of the single-photon pulse. The analogy of the cavity cooperativity C mapped onto the current ring-cavity system is thus

$$C_{\text{ring}} = \frac{g^2}{\Gamma \kappa} = \frac{1}{2\pi} \left(\frac{\lambda}{W} \right)^2 \frac{1}{T}. \tag{43}$$

For $T \ll 1$ and $W \approx \lambda$, we have $C_{\text{ring}} \gg 1$. The present Zeno gate system in this sense also operates in the strong-coupling regime. Seemingly, the Zeno and cavity QED gates would therefore require similar experimental conditions. This conclusion is, however, not necessarily true since the Zeno gates are operated in the regime of $g^2/\Gamma \ll g_c^2/\Gamma_c$ and $\kappa \ll \kappa_c$. The large effective cooperative parameter C_{ring} is merely because the ratio of g^2/Γ to κ remains large. Thus, while cavity QED schemes demand that $g_c \gg \Gamma_c$ and $g_c \gg \kappa_c$ be satisfied simultaneously, the Zeno gate system only relies on $g \sim \Gamma$ and $T \ll 1$. Taking the coherence length of the laser pulse as c/Γ, the condition of $g \sim \Gamma$ would then require the single-photon pulse to be tightly focused down to $W \sim \lambda$, such that

$$\frac{g}{\Gamma} = \sqrt{\frac{1}{2\pi}} \frac{\lambda}{W} \sim 0.1. \tag{44}$$

VIII. FIDELITY UPON HERALDED SUCCESS

In the above discussions, we have considered the reduction in success probability for IFPG and IFRG gates due to imprecise control of atom-photon scattering and/or optics imperfections. In practice, the resulting photon loss can be detected by the absence of the photon at the gate output. By adding a detector to the photon output channel, we find that the detection of a photon necessarily indicates that the device has operated successfully, as all failure mechanisms result in absorption or scattering of the photon out of the resonator mode. Conditioned on this heralded success, the fidelity of the gate operation, measuring the overlap of the target state and the final output state, will be given by $F_{\text{herald}} = \frac{P_{\text{success}}}{1 - P_{\text{decay}}}$. To leading order in $\frac{1}{N}$, F_{herald} is found:

$$F_{\text{herald}} = 1 - |c_{H0}|^2 (|c_{H1}|^2 + |c_{V1}|^2) \frac{(\lambda_0 - \lambda_1)^2}{4} = 1 - O\left(\frac{1}{N^2}\right), \tag{45}$$

compared to $1 - O(\frac{1}{N})$ for the success probability. The small deviation from unity is due to a slight imbalance which occurs in the final normalization of the output state. The fidelity upon heralded success of the present quantum Zeno gates can thus be made extremely close to unity, e.g., for the realistic value $N = 1.5 \times 10^4$ the success probability is 98.4%, yet the corresponding fidelity is 99.994%.

IX. CONCLUSION

In conclusion, we have presented a general theory of interaction- and measurement-free quantum Zeno gates and

discussed their physical implementation via high-finesse optical resonators for systems of single-atom and single-photon qubits. We have constructed a useful set of logic circuits aiming toward quantum-information processing with only one or at most two IFM devices. Because of the interaction- and measurement-free features, as well as the lack of need for preexisting entangled photon pairs, our gates are able to overcome some of the major obstacles in processing information with single photons and atoms. This work is a significant extension and improvement of several previously studied IFM gates [50–52]. We have (1) introduced the interaction-free Raman gate, with which the photon-photon CNOT gate is accomplished using only a single IFM device; (2) constructed the atom-atom and hybrid atom-photon CNOT gate using circuits that are much simpler and easier to implement; (3) constructed direct, reversible atom-photon state transfer circuits; (4) solved the problem of photon loss during long-distance quantum communication via lossy channels with a photon-loss-tolerant protocol. Most importantly, compared to previously studied IFM gates, our gates do not require any measurements and are operated asymptotically on demand. This elimination of measurement clearly distinguishes our Zeno logic gates from previous approaches [1,5,8,11,19,22,50–52,55,62–64]. We have also shown that the success probability and fidelity upon heralded success for our Zeno gates scale at $1 - O(\frac{1}{N})$ and $1 - O(\frac{1}{N^2})$ with N the (effective) number of measurements. Experimentally, N is limited by three major factors, the resonator finesse, the imperfect absorption of the absorbing state, and the imperfect transparency of the transparent state. While the limits to controlling the imperfect absorbtion and transparency factors remain to be investigated, we have shown that with available mirror finesse factors and for realistic atom-photon scattering, a success probability of 98.4% or a fidelity of 99.94% upon heralded success may be attainable in the near future. To this end, we note that, while the present Zeno gates are discussed in the context of single-atomic and -photonic qubits, they can also be implemented in other physical systems in a straightforward manner. A quantum dot system, for example, might be an ideal alternative, due to its large dipole moment as well as the presence of ultrafast phonon-assisted dissipation mechanisms.

APPENDIX A: PURE-STATE REPRESENTATION

In this appendix, we will show that the dynamical evolution of quantum Zeno systems, while involving dissipations into the environment, can nonetheless be described in a pure-state representation with non-Hermitian Hamiltonians. Our analyses are based on the standard quantum treatment of an open system [65], where the dynamics is governed by a master equation for the density matrix. We will take the system with the level scheme drawn in Fig. 1 for an example. Simi-

lar results can be obtained for other systems in a straightforward manner.

With $|g\rangle$ being the atomic state into which the state $|1\rangle$ spontaneously decays, the master equation for this system is read as

$$\dot{\rho} = -\frac{i}{\hbar}[\hat{H}_\Omega, \rho] - \frac{\Gamma}{2}(|1\rangle\langle1|\rho + \rho|1\rangle\langle1| - 2|g\rangle\langle1|1\rho|1\rangle\langle g|).$$
(A1)

Here, ρ is the system's density matrix and Γ is the spontaneous emission rate. The Hamiltonian $\hat{H}_\Omega$, given by Eq. (2), is the Rabi coupling between the states $|0\rangle$ and $|1\rangle$, which, however, does not act on $|g\rangle$. To solve this equation, we expand the density ρ onto the $\{|g\rangle\}$ and $\{|0\rangle, |1\rangle\}$ subspaces, and obtain

$$\rho = \rho_{gg} + \rho_{ss} + \rho_{gs} + \rho_{sg},$$
(A2)

with

$$\rho_{gg} = |g\rangle\langle g|\rho|g\rangle\langle g|,$$

$$\rho_{ss} = \sum_{j,k=0,1} |j\rangle\langle j|\rho|k\rangle\langle k|,$$

$$\rho_{gs} = \rho_{sg}^\dagger = \sum_{j=0,1} |g\rangle\langle g|\rho|j\rangle\langle j|.$$
(A3)

The master equation (A1) can now be separated into three equations:

$$\dot{\rho}_{ss} = -\frac{i}{\hbar}[\hat{H}_\Omega, \rho_{ss}] - \frac{\Gamma}{2}(|1\rangle\langle1|\rho_{ss} + \rho_{ss}|1\rangle\langle1|),$$
(A4)

$$\dot{\rho}_{gg} = \Gamma|g\rangle\langle1|\rho_{ss}|1\rangle\langle g|,$$
(A5)

$$\dot{\rho}_{gs} = \frac{i}{\hbar}\rho_{gs}\hat{H}_\Omega - \frac{\Gamma}{2}\rho_{gs}|1\rangle\langle1|.$$
(A6)

Clearly, Eq. (A4), which governs the motion of ρ_{ss}, is uncoupled from the other equations, meaning that the states $|0\rangle, |1\rangle$ have formed a closed subspace. In this subspace, for any pure initial state $|\Psi(0)\rangle$, Eq. (A4) has a pure-state solution $\rho_{ss}(t) = |\Psi(t)\rangle\langle\Psi(t)|$, where

$$|\Psi(t)\rangle = e^{-i\hat{H}_{\text{eff}}t/\hbar}|\Psi(0)\rangle,$$
(A7)

with $\hat{H}_{\text{eff}}$ defined in Eq. (4). Since our Zeno logic gates are operated in the $\{|0\rangle, |1\rangle\}$ subspace, the state $|g\rangle$ becomes practically irrelevant, allowing us to describe the system in a pure-state representation of $|0\rangle$ and $|1\rangle$ states. $\hat{H}_{\text{eff}}$ is then the effective Hamiltonian governing the pure-state dynamics in this subspace. The system decay is now governed by the non-Hermitian component of $\hat{H}_{\text{eff}}$, due to which the state $|\Psi(t)\rangle$ is no longer normalized to unity. Conservation of probability requires

$$\text{Tr}\{\rho_{gg}\} = 1 - \text{Tr}\{\rho_{ss}\},$$
(A8)

which shows that the reduction in in the normalization of $|\Psi(t)\rangle$ corresponds to the probability for the atom to have scattered into the state $|g\rangle$.

Finally, we note that if we start with an initial state in the $\{|0\rangle, |1\rangle\}$ subspace, the state $|g\rangle$ will always be uncoupled from the rest of the system. This is because the master equation (A1) does not create any coherence between the two subspaces. This can be easily seen from Eq. (A6), where, with zero initial values, the cross terms ρ_{gs}, ρ_{sg} will be identically zero at any later times.

APPENDIX B: DERIVATION OF IFPG PROPAGATOR

In this appendix we will derive the form of the propagator $\hat{V}(\theta, N, \epsilon_0, \epsilon_1)$ that describes the action of the elementary IFPG pictured in Fig. 4. In this system, only the $|V\rangle$ photon interacts with the atom, and the dissipative states exposed to spontaneous emission are $|V0\rangle$ and $|V1\rangle$. The standard master equation describing the dissipative evolution of the system during a single measurement cycle is then [65]

$$\dot{\rho} = \sum_{i=0,1} \frac{\gamma_i}{2}(-|Vi\rangle\langle Vi|\rho - \rho|Vi\rangle\langle Vi| + 2|i\rangle'\langle Vi|\rho|Vi\rangle\langle i|'),$$
(B1)

where the state $|i\rangle'$ describes the scattered atomic qubit state with zero photons in the cavity. The rate constants γ_0 and γ_1 will need to be determined from detailed atom-photon scattering calculations. Following Appendix A, this equation has a pure-state solution in the $\{|H0\rangle, |H1\rangle, |V0\rangle, |V1\rangle\}$ subspace, from which we find that the initial state

$$|\Psi(0)\rangle = c_{H0}|H0\rangle + c_{H1}|H1\rangle + c_{V0}|V0\rangle + c_{V1}|V1\rangle$$
(B2)

evolves into the final state

$$|\Psi(t)\rangle = c_{H0}|H0\rangle + c_{H1}|H1\rangle + c_{V0}e^{-\gamma_0 t/2}|V0\rangle + e^{-\gamma_1 t/2}|V1\rangle.$$
(B3)

The measurement stage of the IFPG corresponds to evolution under (B1) for time t_m such that $e^{-\gamma_0 t_m} \equiv \epsilon_0$ and $e^{-\gamma_1 t_m} \equiv 1 - \epsilon_1$.

With $\hat{B}(\epsilon_0, \epsilon_1)$ as the propagator for the measurement stage and $\hat{R}(\theta, N)$ as the propagator for the rotation stage, the complete IFPG propagator is given by

$$\hat{V}(\theta, N, \epsilon_0, \epsilon_1) = [\hat{B}(\epsilon_0, \epsilon_1)\hat{R}(\theta, N)]^N.$$
(B4)

In the basis $\{|H1\rangle, |V1\rangle, |H0\rangle, |V0\rangle\}$ the matrix forms of the propagators are

$$\hat{R}(\theta,N) = \begin{pmatrix} \cos\dfrac{\theta}{N} & \sin\dfrac{\theta}{N} & 0 & 0 \\[2ex] -\sin\dfrac{\theta}{N} & \cos\dfrac{\theta}{N} & 0 & 0 \\[2ex] 0 & 0 & \cos\dfrac{\theta}{N} & \sin\dfrac{\theta}{N} \\[2ex] 0 & 0 & -\sin\dfrac{\theta}{N} & \cos\dfrac{\theta}{N} \end{pmatrix} \quad \text{(B5)}$$

and

$$\hat{B}(\epsilon_0,\epsilon_1) = \begin{pmatrix} 1 & 0 & 0 & 0 \\ 0 & \sqrt{1-\epsilon_1} & 0 & 0 \\ 0 & 0 & 1 & 0 \\ 0 & 0 & 0 & \sqrt{\epsilon_0} \end{pmatrix}. \quad \text{(B6)}$$

We have found that, to excellent approximation, the full propagator can be expressed as

$$\hat{V}(\theta,N,\epsilon_0,\epsilon_1) = \begin{pmatrix} -\xi_1 & \xi_2 & 0 & 0 \\ -\xi_2 & -\xi_1 & 0 & 0 \\ 0 & 0 & \eta_1 & \eta_2 \\ 0 & 0 & -\eta_3 & -\eta_4 \end{pmatrix}, \quad \text{(B7)}$$

where

$$\xi_1 = e^{-N\epsilon_1/4}, \quad \text{(B8)}$$

$$\xi_2 = (N\epsilon_1/10)^2, \quad \text{(B9)}$$

$$\eta_1 = \left(1 - \frac{\pi^2}{N}\frac{1+\sqrt{\epsilon_0}}{1-\sqrt{\epsilon_0}}\right)^{1/2}, \quad \text{(B10)}$$

$$\eta_2 = \frac{\pi}{N}\left(\frac{1+\sqrt{\epsilon_0}}{1-\sqrt{\epsilon_0}}\right)^{1/2}, \quad \text{(B11)}$$

$$\eta_3 = \pi\sqrt{\epsilon_0}/N, \quad \text{(B12)}$$
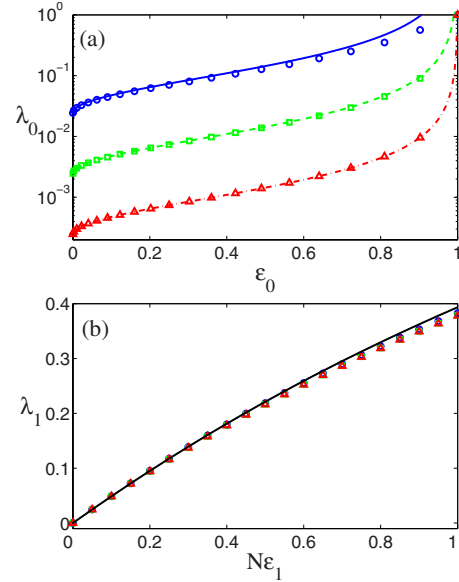
FIG. 11. (Color online) Decay parameters λ_0 and λ_1 versus the atom-photon scattering parameters ϵ_0 and ϵ_1. (a) shows λ_0 versus ϵ_0 for $N=10^2$ (solid line and circles), 10^3 (dashed line and squares), and 10^4 (dashed-dotted line and triangles). All lines are the analytic approximations given in Eq. (38), while the points correspond to exact numerical calculations. In (b) we similarly plot λ_1 versus $N\epsilon_1$, where, because the analytical approximation of λ_1 (39) depends only on the product $N\epsilon_1$, three lines for different N are overlapped. Both figures show excellent agreements between analytic approximations and numerical calculations.

$$\eta_4 = 10\sqrt{\epsilon_0}/N^2. \quad \text{(B13)}$$

The validity of these approximations is illustrated in Fig. 11, where the decay parameters λ_0 and λ_1, given by Eqs. (38) and (39), are plotted against the atom-photon scattering parameters ϵ_0 and ϵ_1. The excellent agreement confirms our conclusions regarding the sensitivity of the success probability and fidelity with respect to the scattering parameters ϵ_0 and ϵ_1.

[1] M. A. Nielsen and I. L. Chuang, *Quantum Computation and Quantum Information* (Cambridge University Press, Cambridge, U.K., 2000).

[2] Q. A. Turchette, C. J. Hood, W. Lange, H. Mabuchi, and H. J. Kimble, Phys. Rev. Lett. **75**, 4710 (1995).

[3] C. Monroe, D. M. Meekhof, B. E. King, W. M. Itano, and D. J. Wineland, Phys. Rev. Lett. **75**, 4714 (1995).

[4] A. Rauschenbeutel, G. Nogues, S. Osnaghi, P. Bertet, M. Brune, J. M. Raimond, and S. Haroche, Phys. Rev. Lett. **83**, 5166 (1999).

[5] E. Knill, R. Laflamme, and G. J. Milburn, Nature (London) **409**, 46 (2001).

[6] K. J. Resch, J. S. Lundeen, and A. M. Steinberg, Phys. Rev. Lett. **89**, 037904 (2002).

[7] D. Leibfried, B. DeMarco, V. Meyer, D. Lucas, M. Barrett, J. Britton, W. M. Itano, B. Jelenković, C. Langer, T. Rosenband, and D. J. Wineland, Nature (London) **422**, 412 (2003).

[8] T. B. Pittman, M. J. Fitch, B. C. Jacobs, and J. D. Franson, Phys. Rev. A **68**, 032316 (2003).

[9] T. Yamamoto, Yu. A. Pashkin, O. Astafiev, Y. Nakamura, and J. S. Tsai, Nature (London) **425**, 941 (2003).

[10] J. L. O'Brien, G. J. Pryde, A. G. White, T. C. Ralph, and D. Branning, Nature (London) **426**, 264 (2003).

[11] P. Kok, W. J. Munro, K. Nemoto, T. C. Ralph, J. P. Dowling, and G. J. Milburn, Rev. Mod. Phys. **79**, 135 (2007) and references therein.

[12] D. Bouwmeester, J. W. Pan, K. Mattle, M. Eibl, H. Weifurter, and A. Zeilinger, Nature (London) **390**, 575 (1997).

[13] C. Z. Peng, T. Yang, X. H. Bao, J. Zhang, X. M. Jin, F. Y. Feng, B. Yang, J. Yang, J. Yin, Q. Zhang, N. Li, B. L. Tian, and J.-W. Pan, Phys. Rev. Lett. **94**, 150501 (2005).

[14] T.-Y. Chen, J. Zhang, J.-C. Boileau, X.-M. Jin, B. Yang, Q. Zhang, T. Yang, R. Laflamme, and J.-W. Pan, Phys. Rev. Lett. **96**, 150504 (2006).

[15] W. Tittel, J. Brendel, H. Zbinden, and N. Gisin, Phys. Rev. Lett. **84**, 4737 (2000).

[16] S. L. Braunstein and H. J. Kimble, Phys. Rev. A **61**, 042302 (2000).

[17] M. W. Mitchell, J. S. Lundeen, and A. M. Steinberg, Nature (London) **429**, 161 (2004).

[18] I. Marcikic, H. de Riedmatten, W. Tittel, H. Zbinden, and N. Gisen, Nature (London) **421**, 509 (2003).

[19] S. Bose, P. L. Knight, M. B. Plenio, and V. Vedral, Phys. Rev. Lett. **83**, 5158 (1999).

[20] S.-B. Zheng and G.-C. Guo, Phys. Rev. A **73**, 032329 (2006).

[21] L.-M. Duan and H. J. Kimble, Phys. Rev. Lett. **90**, 253601 (2003).

[22] T. Di, A. Muthukrishnan, M. O. Scully, and M. S. Zubairy, Phys. Rev. A **71**, 062308 (2005).

[23] M. Riebe, H. Häffner, C. F. Roos, W. Hänsel, J. Benhelm, G. P. T. Lancaster, T. W. Körber, C. Becher, F. Schmidt-Kaler, D. F. V. James, and R. Blatt, Nature (London) **429**, 734 (2004).

[24] M. D. Barrett, J. Chiaverini, T. Schaetz, J. Britton, W. M. Itano, J. D. Jost, E. Knill, C. Langer, D. Liebfried, R. Ozeri, and D. J. Wineland, Nature (London) **429**, 737 (2004).

[25] N. A. Gershenfeld and I. L. Chuang, Science **275**, 350 (1997).

[26] L.-M. Duan, J. I. Cirac, P. Zoller, and E. S. Polzik, Phys. Rev. Lett. **85**, 5643 (2000).

[27] Y. P. Huang and M. G. Moore, Phys. Rev. A **77**, 032349 (2008).

[28] A. D. Boozer, A. Boca, R. Miller, T. E. Northup, and H. J. Kimble, Phys. Rev. Lett. **97**, 083602 (2006).

[29] A. D. Boozer, A. Boca, R. Miller, T. E. Northup, and H. J. Kimble, Phys. Rev. Lett. **98**, 193601 (2007).

[30] B. Julsgaard, A. Kozhekin, and E. S. Polzik, Nature (London) **413**, 400 (2001).

[31] D. N. Matsukevich and A. Kuzmich, Science **306**, 663 (2004).

[32] A. Beige, D. Braun, B. Tregenna, and P. L. Knight, Phys. Rev. Lett. **85**, 1762 (2000).

[33] B. Misra and E. C. G. Sudarshan, J. Math. Phys. **18**, 756 (1977).

[34] A. Peres, Am. J. Phys. **48**, 931 (1980).

[35] E. Joos, Phys. Rev. D **29**, 1626 (1984).

[36] W. M. Itano, D. J. Heinzen, J. J. Bollinger, and D. J. Wineland, Phys. Rev. A **41**, 2295 (1990).

[37] S. H. Simon and P. M. Platzman, Phys. Rev. A **61**, 052103 (2000).

[38] J. Ruseckas and B. Kaulakys, Phys. Rev. A **73**, 052101 (2006).

[39] T. Tsegaye, E. Goobar, A. Karlsson, G. Björk, M. Y. Loh, and K. H. Lim, Phys. Rev. A **57**, 3987 (1998).

[40] P. Kwiat, H. Weinfurter, and A. Zeilinger, Sci. Am. **2755**, 72 (1996).

[41] A. G. White, J. R. Mitchell, O. Nairz, and P. G. Kwiat, Phys. Rev. A **58**, 605 (1998).

[42] P. G. Kwiat, A. G. White, J. R. Mitchell, O. Nairz, G. Weihs, H. Weinfurter, and A. Zeilinger, Phys. Rev. Lett. **83**, 4725 (1999).

[43] T. Rudolph, Phys. Rev. Lett. **85**, 2925 (2000).

[44] A. C. Elitzur and L. Vaidman, Found. Phys. **23**, 987 (1993).

[45] P. G. Kwiat, H. Weinfurter, T. Herzog, A. Zeilinger, and M. A. Kasevich, Phys. Rev. Lett. **74**, 4763 (1995).

[46] P. Horodecki, Phys. Rev. A **63**, 022108 (2001).

[47] L.-M. Duan and G.-C. Guo, Phys. Rev. A **58**, 3491 (1998).

[48] P. Zanardi and F. Rossi, Phys. Rev. B **59**, 8170 (1999).

[49] S. Pötting, E. S. Lee, W. Schmitt, I. Rumyantsev, B. Mohring, and P. Meystre, Phys. Rev. A **62**, 060101(R) (2000).

[50] A. Gilchrist, A. G. White, and W. J. Munro, Phys. Rev. A **66**, 012106 (2002).

[51] H. Azuma, Phys. Rev. A **68**, 022320 (2003).

[52] H. Azuma, Phys. Rev. A **70**, 012318 (2004).

[53] J. D. Franson, B. C. Jacobs, and T. B. Pittman, Phys. Rev. A **70**, 062302 (2004).

[54] O. Hosten, M. T. Rakher, J. T. Barreiro, N. A. Peters, and P. G. Kwiat, Nature (London) **439**, 949 (2006).

[55] T. C. Ralph, A. G. White, W. J. Munro, and G. J. Milburn, Phys. Rev. A **65**, 012314 (2001).

[56] C. H. Bennett, G. Brassard, C. Crépeau, R. Jozsa, A. Peres, and W. K. Wootters, Phys. Rev. Lett. **70**, 1895 (1993).

[57] M. A. Nielsen, E. Knill, and R. Laflamme, Nature (London) **396**, 52 (1998).

[58] A. Kuzmich and E. S. Polzik, Phys. Rev. Lett. **85**, 5639 (2000).

[59] N. Takei, H. Yonezawa, T. Aoki, and A. Furusawa, Phys. Rev. Lett. **94**, 220502 (2005).

[60] A. Dantan, N. Treps, A. Bramati, and M. Pinard, Phys. Rev. Lett. **94**, 050502 (2005).

[61] J. M. Raimond, M. Brune, and S. Haroche, Rev. Mod. Phys. **73**, 565 (2001) and references therein.

[62] T. C. Ralph, N. K. Langford, T. B. Bell, and A. G. White, Phys. Rev. A **65**, 062324 (2002).

[63] H. F. Hofmann and S. Takeuchi, Phys. Rev. A **66**, 024308 (2002).

[64] Z. Zhao, A.-N. Zhang, Y.-A. Chen, H. Zhang, J.-F. Du, T. Yang, and J.-W. Pan, Phys. Rev. Lett. **94**, 030501 (2005).

[65] P. Meystre, *Atom Optics* (Springer, New York, 2001).